THE JOURNAL OF PHYSICAL CHEMISTRY B

Article

pubs.acs.org/JPCB

Adsorption Behavior of Hydrophobin Proteins on Polydimethylsiloxane Substrates

Yingzhe Liu,[†] Ming Wu,[‡] Xizeng Feng,[‡] Xueguang Shao,[†] and Wensheng Cai*,[†]

[†]College of Chemistry, Nankai University, Tianjin, 300071, People's Republic of China

[‡]College of Life Science, Nankai University, Tianjin, 300071, People's Republic of China

Supporting Information

ABSTRACT: The design of a bioactive surface with appropriate wettability for effective protein immobilization has attracted much attention. Previous experiments showed that the adsorption of hydrophobic protein HFBI onto a polydimethylsiloxane (PDMS) substrate surface can reverse the inherent hydrophobicity of the surface, hence making it suitable for immobilization of a secondary protein. In this study, atomistic molecular dynamics simulations have been conducted to elucidate the adsorption mechanism of HFBI on the PDMS substrate in an aqueous environment. Nine independent simulations starting from three representative initial orientations of HFBI toward the solid surface were performed, resulting in different adsorption modes. The main secondary structures of the protein in each mode are found to be preserved in the entire course of adsorption due to the four disulfide bonds. The relative binding free energies of the different adsorption modes were calculated, showing that the mode, in which the binding residues of HFBI fully come from its hydrophobic patch, is most energetically favored. In this favorable binding mode, the hydrophilic region of HFBI is fully exposed to water, leading to a high hydrophilicity of the modified PDMS surface, consistent with experiments. Furthermore, a set of residues consisting of Leu12, Leu24, Leu26, Ile27, Ala66, and Leu68 were found to play an important role in the adsorption of HFBI on different hydrophobic substrates, irrespective of the structural features of the substrates.

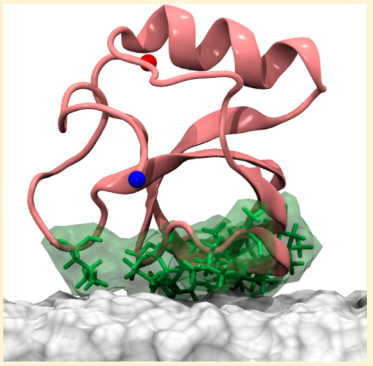

1. INTRODUCTION

Biomolecule immobilization on solid substrates plays an important role in many biological investigations, such as protein microarrays, molecular recognition, and enzymology, offering a wide spectrum of applications that range from proteomic profiling and diagnostics and biosensors to chemical manufacturing and nanoarchitecture.[1] The design of bioactive solid surfaces with appropriate wettability for effective immobilization, therefore, is of paramount concern.

Hydrophobins are small amphiphilic proteins naturally produced by filamentous fungi, which have been the object of an increasing interest for surface modification on account of their intrinsic biocompatibility and remarkable structural features. On account of the extraordinary surface activity, hydrophobins can self-assemble into an amphipathic membrane at hydrophilic−hydrophobic interfaces and consequently modify the characteristics of the surface to which they attach. Therefore, they can act as an intermediate to immobilize biomolecules, including fusion proteins,[2] lipases,[3] enzymes,[4] and antibodies,[5] resulting in a broad potential in biosensors and drug delivery.[6] Besides, hydrophobins can even prevent secondary protein adsorption[7] and immune recognition of airborne fungal spores.[8] Experiments show that hydrophobins can adsorb onto hydrophobic surfaces to form ordered films with highly regular patterns.[9−11] On the basis of this structural feature, hydrophobins can be used as building blocks to synthetize novel nanoscale structures and materials.[12,13] More details and applications on hydrophobins have been reviewed by Hektor, Scholtmeijer, and Linder.[14,15]

Hydrophobins are able to modify diverse surfaces of inorganic materials, for example, carbon nanotubes,[12] graphene,[16] mica,[17] silicon substrates,[9] etc. As a kind of optical transparent, elastic, and nontoxic polymer, polydimethylsiloxane (PDMS) has been widely used in microfluidic devices.[18] Advancement in direct immobilization of biomolecules onto the PDMS surface has, however, been severely impeded as a result of its inherent hydrophobicity. Although some approaches, such as ultraviolet oxidation,[19] can overcome this shortcoming, the chemical modifications inevitably give rise to physical damage to the surface properties. Most importantly, the lower biocompatibility of PDMS greatly limits its further applications in biological and medical fields.

Recently, it has been reported that adhesion of an HFBI assembly, one kind of hydrophobin from *Trichoderma reesei*, on a PDMS substrate can reverse the wettability of the surface, from hydrophobic to hydrophilic. The modified surface is suitable for immobilization of a secondary protein, that is, chicken immunoglobulin.[17,20] This convenient and rapid method for bioactive surface modification may have potential applications in immunoassays, biosensors, and microfluidic

Received: May 17, 2012
Revised: August 29, 2012
Published: September 19, 2012

dx.doi.org/10.1021/jp304796p | *J. Phys. Chem. B* 2012, 116, 12227−12234

networks. However, details of the microscopic structure, the physical properties, and the adsorption mechanism of HFBI on the solid surface are still fragmentary.

Theoretical explorations, particularly molecular dynamics (MD) simulations, have been endeavored to decipher the mechanism through which proteins and surfaces/interfaces interact.[21,22] Much information, including protein orientation, conformational changes, key residues, and driving forces, has been obtained from simulations of adsorption of hydrophobins on bare silicon and graphite surfaces.[23,24] In addition to adsorption, the folding of hydrophobins at different hydrophobic/hydrophilic interfaces was investigated.[25,26]

In the present contribution, the nature of the interplay between hydrophobin HFBI and the hydrophobic surface of PDMS is probed employing MD simulations to help interpret the available experiments.[17,20] The following interesting issues are aimed to be addressed: (1) What is the favorable adsorption mode? (2) What are the important residues of HFBI for the adsorption? (3) How does the conformation of the protein change during the adsorption process? (4) What is the adsorption mechanism (the driving force)?

2. METHODS

2.1. Molecular Models. *HFBI.* The initial coordinates of HFBI were taken from the tetrameric crystal structure[27] available in the protein data bank (PDB code: 2FZ6). The monomer A was extracted out, and three missing residues, that is, Ser1, Gly74, and Ala75, were repaired using the program Swiss-PdbViewer.[28] Four disulfide bonds were retained. Subsequently, this molecular model was sufficiently relaxed in an explicit water environment by an equilibrium simulation of 10 ns. The rmsd values of the HFBI backbone fluctuate around 1 Å as a function of time, suggesting that the protein is stable in the aqueous medium, and the hydrophobic patch composed of residues Leu12, Val23, Leu24, Leu26, Ile27, Leu29, Val59, Ala60, Val62, Ala63, Ala66, Leu67, and Leu68 can also be preserved (the simulation details and results can be found in the Supporting Information). The equilibrium structure of HFBI was then applied as an initial conformation for the simulations of protein adsorption (see Figure 1).

PDMS. The chemical formula for PDMS is $Si(CH_3)_3O[Si(CH_3)_2O]_nSi(CH_3)_3$, where n is the number of repeat units. It was reported that the wettability of PDMS surfaces is independent of the PDMS chain length by comparing the 20-unit length with the 100-unit length.[29] Therefore, the initial model of a linear 20-unit PDMS chain was constructed. First, the single PDMS chain was fully equilibrated in the gas phase for 10 ns. Twelve conformations of the PDMS chain extracted from the trajectory of the last 2.4 ns at an interval of 200 ps were then reoriented and arranged into an array of 3 × 4 points. Second, the array was compressed into a slab of 55 × 55 × 11 $Å^3$ corresponding to the experimental density by means of tclBC forces implemented with NAMD2.7.[30] Finally, equilibration of the nonboundary surface keeping the same density was performed using periodic boundary conditions (PBCs).

Herein, all the atoms of the nonboundary solid substrate were frozen. The length of the simulation box in the direction of the Z axis is long enough, that is, about 85 Å, to avoid possible direct contact between HFBI and the image of substrates. Sodium and chloride ions were added randomly, corresponding to the physiological concentration, that is, 0.15 $mol·L^{-1}$ (see Figure 1). Furthermore, three representative initial orientations of HFBI toward the PDMS surface were

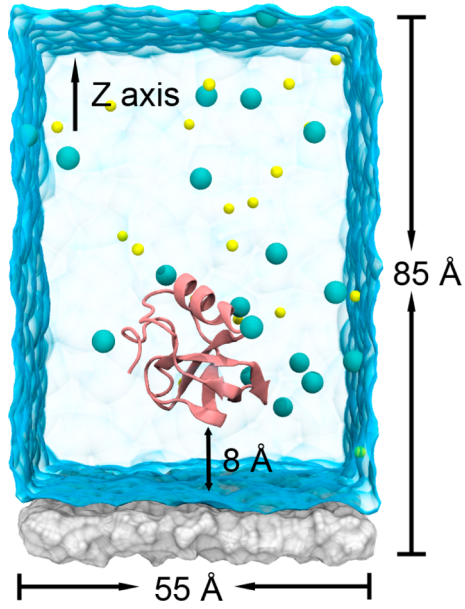

Figure 1. Initial structure of the molecular system for the adsorption simulation of HFBI on the PDMS surface. HFBI is represented by the new cartoon style and colored in pink. Sodium and chloride ions are highlighted by yellow and cyan spheres, respectively.

taken into account (see Figure 2). The nearest distance between HFBI and the substrate surface was set to 8 Å so that HFBI could adopt the suitable orientation to interact with the solid surface by rotational and translational motions. However, it may give rise to free diffusion of HFBI and nonadsorption on the substrate surface. Therefore, three independent simulations were performed for each initial orientation to enlarge the sampling space. The general description of the molecular systems considered in this study is summarized in Table S1 (see the Supporting Information).

2.2. Molecular Dynamics Simulations. All the MD simulations described herein were carried out using the program NAMD2.7[30] in the isobaric−isothermal ensemble with PBCs applied in three directions of Cartesian space. The CHARMM27 force field[31,32] and the TIP3P model[33] were employed for hydrophobin HFBI and water molecules, respectively. The parameters of PDMS were taken from the available literature,[34] and the atomic partial charges were taken from quantum chemistry calculations.[35] After the equilibration simulation of the PDMS substrate, hydrogen and carbon atoms are found to be primarily located on the surface, which is similar to the findings of recent MD simulations.[36]

The temperature and the pressure were maintained at 300 K and 1 atm, respectively, employing Langevin dynamics and the Langvein piston method.[37] To keep the nonboundary solid surface, the pressure fluctuation was allowed only in the direction of the Z axis. The equations of motion were integrated using the multiple time-step Verlet r-RESPA algorithm[38] with time steps of 2 and 4 fs for short- and long-range interactions, respectively. Covalent bonds involving hydrogen atoms were constrained to their equilibrium lengths by virtue of the SHAKE/RATTLE algorithms.[39,40] Long-range electrostatic forces were evaluated employing the particle mesh Ewald (PME) approach,[41] and a smoothed 12 Å spherical cutoff was used to truncate van der Waals interactions. Each molecular system before production simulation underwent 5000 steps of energy minimization, 5 ps of heating from 0 to

dx.doi.org/10.1021/jp304796p | J. Phys. Chem. B 2012, 116, 12227−12234

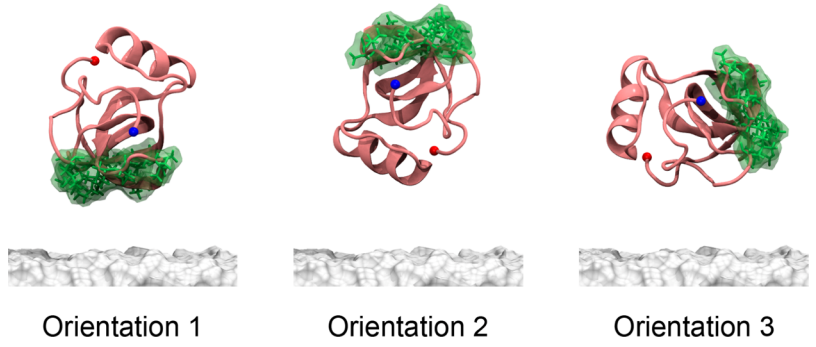

Figure 2. Three representative orientations are denoted as orientation 1, 2, and 3, indicating the hydrophobic patch of HFBI facing the substrates, back to the substrates, and vertical to the substrates. HFBI is represented by the new cartoon style, and the hydrophobic patch is colored in lime. The N and C termini are highlighted by blue and red spheres, respectively. For clarity, water molecules and ions are removed.

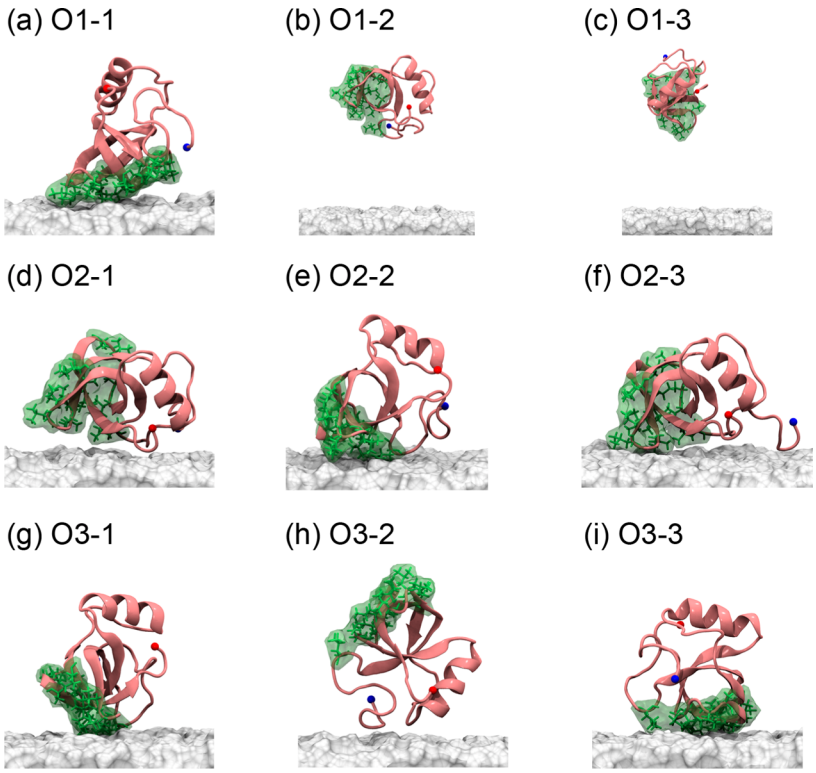

Figure 3. Final snapshots of molecular systems obtained from the 50 ns trajectories, excluding water and ions for clarity. Three independent simulations with (a–c) orientation 1, (d–f) orientation 2, and (g–i) orientation 3. The drawing and coloring are the same as those in Figure 2.

300 K, and then 100 ps of water equilibration. Visualization and analysis of MD trajectories were performed with the VMD package.[42]

2.3. Molecular Mechanics Poisson–Boltzmann Surface Area (MM-PBSA) Calculations. The MM-PBSA approach combines an explicit molecular mechanical model for the solute with a continuum description of the solvent to estimate the free energy of a complex system.[43] It requires a set of representative structures sampled by MD simulations, and postprocessing of these structures. The binding free energy can be calculated by comparison of the complexed trajectory with separate trajectories of the acceptor and ligand. In this method, the free energy of each unbound molecule is given by the following equation

$$G = E_{MM} + G_{solv} - TS_{conf} \quad (1)$$

where E_{MM} is the molecular mechanics energy of the solute in the gas phase, composed of the bond, angle, torsion, van der Waals, and electrostatic terms. The solvation free energy, G_{solv}, can be further split into a polar (electrostatic), G_{PB}, and nonpolar (hydrophobic) part, G_{NP}. The last term in the above equation is the solute entropy. This term is likely to be much smaller than the other two terms in many applications of estimating relative free energies.[43] The binding free energy can be obtained by the difference

$$\Delta G_{bind} = G_{complex} - G_{receptor} - G_{ligand} \quad (2)$$

In the present work, the MM-PBSA method was employed to compare the relative binding affinities of HFBI and PDMS among different adsorption modes. These adsorption modes were obtained from the 50 ns MD simulations of the same molecular system only with different initial orientations. The entropic terms are supposed to be similar for these adsorption

dx.doi.org/10.1021/jp304796p | J. Phys. Chem. B 2012, 116, 12227–12234

modes. Hence, their contributions to the relative binding affinities were ignored in this study. Furthermore, the free energies of HFBI and PDMS are the same for all the molecular systems. Therefore, the relative binding affinities of different adsorption modes can be compared by the free energy of the complexes.

The MM-PBSA analysis was performed using the same force field employed in the MD simulations for the MM contribution and APBS[44] for the Poisson−Boltzmann contribution. For the APBS calculation, the iAPBS[45] interface was used to call APBS from NAMD. Thereinto, the protein dielectric was set to 1.0, the solvent dielectric was set to 80.0, the solvent radius was set to 1.4 Å, the grid spacing was 0.5 Å in each dimension, and the rest of the parameters were default values. Here, only the trajectories of the last 10 ns were used for MM-PBSA calculation.

3. RESULTS AND DISCUSSION

3.1. Conformations of HFBI on the Solid Surface. Adsorption of HFBI on the PDMS surface was observed in seven out of the nine 50 ns MD simulations, whereas it did not occur in the other two runs within the time scale explored. The final structures of the molecular system obtained from the nine trajectories are shown in Figure 3. For convenience, each simulation is labeled with a prefix of the orientation, followed by the simulation number. For example, O1-1 means the first simulation with orientation 1. In the following discussion, only the seven trajectories where the adsorption occurred were analyzed.

To investigate the motion of HFBI during the adsorption process, the centroid distance between the protein and PDMS was monitored as a function of time. As shown in Figure 4a, for

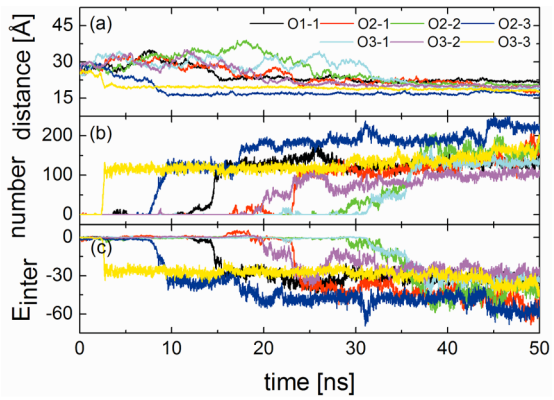

Figure 4. (a) Center-of-mass distance between HFBI and PDMS as a function of simulation time. (b) The number of atoms of HFBI within 6 Å around the surface of PDMS in the course of the adsorption process. (c) Time evolution of the interaction energy (kcal/mol) of HFBI and PDMS.

the systems O2-3 and O3-3, the distances decrease rapidly in 10 ns and then become stable. In contrast, for the rest of the systems, the distances initially increase and then decrease to stable values. Furthermore, the number of the adsorbed atoms, that is, within 6 Å around the PDMS surface, was calculated in the course of adsorption. It can be seen clearly from Figure 4b, for the O3-3 system, the number increases rapidly and reaches a plateau after ca. 3 ns, indicating that HFBI can quickly adsorb on the solid surface. For some systems like O2-3, this number rises in a stepwise manner, demonstrating that HFBI adjusts its structure gradually after initial adsorption and tends to bind to the PDMS surface through contacting with more interfacial atoms. In addition, the interaction energy profiles of HFBI and PDMS (see Figure 4c) are almost symmetric with those in Figure 4b. It can be proved that the interactions mainly depend on the contacting atoms at the interface. Moreover, van der Waals interactions are shown to be predominant (see Table S2, Supporting Information). The interaction energies decrease in the initial stage of the simulations, and level off in the last stage, indicative of a convergence of the adsorption simulations. It can be, therefore, concluded that van der Waals attractions constitute the main driving force responsible for the initial adsorption.

The structural stability of the hydrophobin was examined by the rmsd of the heavy atoms of HFBI. The rmsd values of the O3-1 and O3-3 systems are the lowest (ca. 1.4 Å), suggestive of no significant conformational changes. In contrast, the rmsd of system O2-3 goes up to ca. 4 Å, arising from a large structural deformation. These structural changes mainly come from the flexible turn and coil close to the N-terminal part of HFBI. The rmsf value of the N terminus for system O3-3 is the lowest, whereas that value for the system O2-3 is up to ca. 8 Å. In addition to the N-terminal part, the region between residues 60 and 70 shows a larger flexibility than the other parts of HFIB, in particular, for system O2-2 (see the Supporting Information).

Details of the structural change as a function of time are provided in the Supporting Information (Figure S4). The main secondary structures, such as the α helix and β sheet, were preserved in the course of adsorption, which accords with the experimental results.[9,46] It can be attributed to the four strong disulfide bonds. Besides, a general structural transformation from a coil to a turn structure between residues 60 and 66 was observed. The same region was found to have a local structural rearrangement in the process of multimer formation.[27] In the crystal structure of the HFBI tetramers, the structure of monomer D in this region is more extended than that of monomer A, leading to a rugged morphology of the hydrophobic patch, which may reduce the interaction of the hydrophobic patch and the PDMS surface. Another 100 ns equilibration simulation of monomer D in solution shows that the flexible loop 60−66 can regulate its conformation and shrink back to a flat hydrophobic patch like monomer A. Therefore, it can be conjectured that the structural difference of loop 60−66 among the HFBI monomers may not lead to different adsorption behaviors on PDMS. For monomer A, however, is the conformational change between residues 60 and 66 induced by the PDMS surface? To answer this question, the equilibration simulation of monomer A alone was prolonged from 10 to 100 ns. The results show that the region of 60−66 is very flexible and has an obvious structural change from 50 to 80 ns, suggesting that the conformational change of this region is irrespective of the presence of the PDMS surface (the analysis results can be found in the Supporting Information).

Additionally, an interesting structural transformation of the region near the N terminus was found for system O2-3, from turn to coil and then back to turn. From the simulation results of monomer A alone in water, it can be concluded that this structural change cannot happen in the absence of the PDMS substrate, although the region near the N terminus is flexible. Analysis of the MD trajectory shows that this region extended from the whole protein by means of the structural change from turn to coil, and then gradually adsorbed on the PDMS surface, followed by changing back to the turn structure. Hence, it is

reasonable to infer that the structural transformation helps the adsorption process through favorable van der Waals interactions.

The overall size of HFBI was monitored in the adsorption process by calculating the radius of gyration (R_g). An expansion of the size of HFBI is observed after the adsorption in all the molecular systems. The O3-3 system is found to possess the smallest R_g of ca. 10.8 Å, whereas the O2-3 system has the largest R_g close to 12 Å. Moreover, the overall shape of HFBI is characterized by the eccentricity, which is defined as $1 - I_{ave}/I_{max}$, where I_{max} is the maximal principal moment of inertia and I_{ave} is the average of three principal moments of inertia. The eccentricity is zero for a perfect sphere and close to 1 for a flat or needlelike ellipsoid. The average eccentricities of systems O1-1, O2-1, O2-2, O2-3, O3-1, O3-2, and O3-3 during the last 10 ns trajectories are 0.18, 0.18, 0.20, 0.19, 0.17, 0.17, and 0.16, respectively, indicating that the shape of HFBI after absorption is close to a sphere for different absorption modes. The orientation of HFBI was monitored in the course of adsorption. For system O3-3, the cosine of the orientation angle changes from 0 to −1 in the first 5 ns, suggesting that HFBI can quickly adsorb on the PDMS surface through suitable rotation and translation without large conformational changes (see Figure S2 in the Supporting Information).

3.2. Adsorption Modes and Key Residues. Different adsorption conformations of the hydrophobin on the solid surface were obtained and are shown in Figure 3. On the basis of the interaction sites between the hydrophobic patch and the PDMS surface, adsorptions modes can be classified into four classes. First, for system O3-3, almost the entire hydrophobic patch is buried. Second, for systems O1-1, O2-2, and O3-1, only part of the hydrophobic patch directly interacts with the PDMS surface. Third, for system O2-3, the adsorption sites are composed of part of the hydrophobic patch and the residues near the N and C termini. Finally, for systems O2-1 and O3-2, the hydrophobic patch is fully exposed to the solvent. Furthermore, the degree of the hydrophobic patch buried by the PDMS surface is characterized by its solvent-accessible surface area (SASA). As shown in Figure 5, the SASA of the hydrophobic patch for system O3-3 is the smallest, implying that the corresponding buried area by PDMS is the largest. Not surprisingly, the corresponding SASAs for systems O2-1 and O3-2 are the highest on account of the full exposure of the hydrophobic patch.

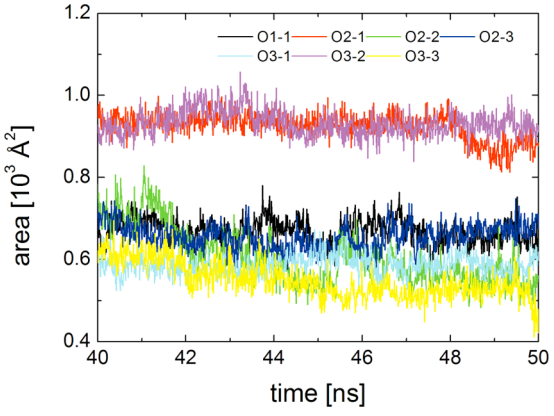

Figure 5. SASA of the hydrophobic patch during the last 10 ns trajectories.

To investigate the optimal adsorption mode, the relative binding free energies between HFBI and PMDS were calculated by means of the MM-PBSA method and are displayed in Table 1. For system O3-2, HFBI interacts with the PDMS surface mainly through the residues near the N terminus, and the hydrophobic patch is fully exposed to the solvent environment. This binding mode, therefore, possesses the highest binding free energy and is taken as a reference. It can be found that the contribution of ΔG_{NP} can be basically ignored and the most differences of the binding free energies come from the ΔE_{MM} and ΔG_{PB} terms. For system O3-3, the structural change of HFBI after adsorption is minimal, leading to the lowest ΔE_{MM}. Besides, the polar solvation free energy is favorable because a very large proportion of the hydrophobic patch is buried. Therefore, the adsorption mode is energetically favored and stable. This interaction mechanism and structural feature of HFBI can interpret the dramatic change of the water contact angle observed in experiment.[17] The water contact angle of a bare PDMS surface is measured to be 123.9°, while it becomes 51.0° after the adsorption of HFBI. The native hydrophobicity of PDMS is reversed dramatically because the hydrophobic surface of PDMS is coated with HFBI by the hydrophobic patch and the hydrophilic segment of HFBI is exposed to the aqueous environment. Therefore, this bioactive solid surface with appropriate wettability can be applied to the effective immobilization of proteins.

Table 1. Summary of MM-PBSA Results[a]

system	ΔE_{MM}[c]	ΔG_{PB}	ΔG_{NP}	ΔG
O1-1	13	−67	0	−54
O2-1	15	−70	−4	−59
O2-2	26	−110	−3	−87
O2-3	10	−104	−10	−104
O3-1	−36	−137	−6	−179
O3-2[b]	0	0	0	0
O3-3	−58	−131	−9	−198

[a]All results are in kcal/mol. The relative standard errors are not more than 0.02 and calculated by block averaging, in which the last 10 ns trajectories were divided into four segments. [b]The system O3-2 was defined as a reference state. [c]ΔE_{MM} energies include not only the noncovalent interactions of HFBI and PDMS but also the change of the conformational energies of HFBI.

All the binding modes except O3-3 correspond to local minima in the free-energy landscape, which may be caused by kinetic trapping at room temperatures. The transition from these modes to the energetically favored one (O3-3) is particularly difficult within the time scale explored, on account of insufficient sampling or an insurmountable energy barrier.

Combining the relative binding free energies and the SASA of the hydrophobic patch of HFBI (Figure 5), it can be seen that hydrophobic interactions of the hydrophobic patch and PDMS play an important role to stabilize adsorption. In experiments, long-term stability is crucial for the adsorbed complex, particularly when exposed to the air. Therefore, the MD simulation of system O3-3 was prolonged from 50 to 100 ns to investigate the stability of the HFBI:PDMS complex in the aqueous environment. The result shows that main secondary structures of HFBI, such as the α helix and β sheet, were preserved during the 100 ns trajectory. Furthermore, the orientation angle of HFBI is very steady in the extra trajectory of 50 ns, suggestive of a stable adsorption.

dx.doi.org/10.1021/jp304796p | J. Phys. Chem. B 2012, 116, 12227−12234

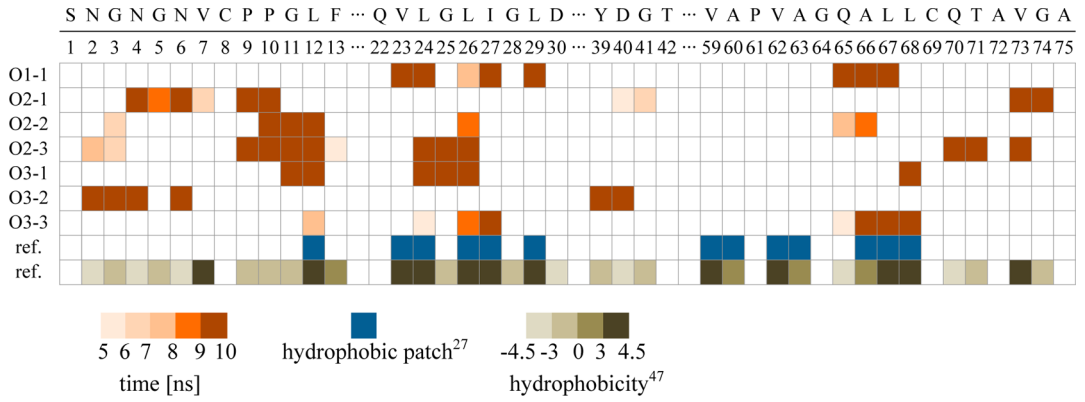

Figure 6. Adsorbed residues in the last 10 ns trajectory are colored in terms of their residence time on the surface. Here, the adsorbed residues are defined as the residues with their centroids within 6 Å around the solid surface.

Subsequently, the final structure of the absorbed complex was equilibrated in the gas phase for 30 ns to explore its stability when exposed to the air. The simulation results suggest that the structure of HFBI was adjusted slightly but the adsorption conformation is still stable with the adsorbed residues derived from the hydrophobic patch (see Figures S5 and S6 in the Supporting Information).

To explore the key residues responsible for the adsorption modes, the adsorbed residues along with their residence time on the surface were figured out and are depicted in Figure 6. For systems O2-1 and O3-2, the adsorbed residues are basically composed of hydrophilic residues, giving rise to the unfavorable desolvation energies. From the analysis of the adsorbed residues in the seven molecular systems, it can be found that Leu12, Leu24, Leu26, and Ala66 are frequently present in the adsorption of HFBI through the hydrophobic patch, indicative of the importance of these residues for the adsorption. It is an interesting issue to address if these residues are also crucial for the adsorption of HFBI on other hydrophobic surfaces.

Previous MD simulations[24] showed that Leu12, Leu26, Leu27, Val62, Ala66, and Leu68 are the interfacial residues for the interactions of HFBI and a graphite surface. These residues except Val62 are also found in the interface of HFBI/PDMS in system O3-3. In our other study about the adsorption of HFBI on single-walled carbon nanotubes (SWCNTs),[48] the adsorbed residues are Leu26, Ile27, Val59, Ala60, Val62, Ala66, Leu67, and Leu68. The common residues found in the three interfaces (HFBI/PDMS, HFBI/graphite, and HFBI/SWCNT) are, therefore, Leu26, Ile27, Ala66, and Leu68, indicating that they play a significant role in the adsorption of HFBI. Combining the above analyses, we can propose a set of key residues, that is, Leu12, Leu24, Leu26, Ile27, Ala66, and Leu68. These residues govern the adsorption of HFBI on different hydrophobic surfaces, PDMS substrates, graphite surfaces, and SWCNTs. Hence, it can be inferred that the adsorption behavior of HFBI on a hydrophobic surface is mainly related to the hydrophobic patch of the protein and almost irrespective of the structural feature of the surface.

In addition to HFBI, bovine serum albumin (BSA) can be applied as an anchor layer for protein immobilization on the PDMS surface.[49] These two surface modification methods, however, have different interaction mechanisms and advantages. Owing to its amphiphilic structural feature, HFBI can adsorb on the native PDMS surface by its hydrophobic patch while its hydrophilic region is exposed to the aqueous environment, which changes the surface wettability to hydrophilicity. Besides, HFBI can modify the superhydrophilic surface of a mica substrate, leading to a moderately hydrophilic surface.[17] Hence, HFBI adsorption may be a versatile and convenient method for the immobilization of biomolecules on diverse substrates. For the BSA modification method, polyelectrolyte multilayers are added between the PDMS surface and BSA to provide long-term hydrophilic stability. Furthermore, the BSA anchor layer can successfully reduce nonspecific binding and enhance binding affinity. The long-term affinity can be conserved for at least 7 days in its dry form. From the above discussion, it can be found that different proteins as the anchor layer for PDMS can provide different features and advantages, such as the structural features of proteins, stability, and specific binding. Therefore, these characteristics should be considered in choosing proteins to modify hydrophobic substrates.

4. CONCLUSION

A series of atomistic MD simulations have been performed to explore the adsorption mechanism of HFBI on the PDMS surface. The binding free energies for different adsorption conformations obtained from nine independent MD runs were calculated employing the MM-PBSA method. The results show that, for the most energetically favored adsorption mode, the binding site of HFBI is fully located in its hydrophobic patch. This adsorption mode has a stable adsorption structure and a favorable solvation free energy, which can explain the regular orientation of the hydrophobin and the high hydrophilicity of the modified PDMS surface after adsorption found in experiments. The main secondary structures of HFBI persevered in the entire course of the adsorption due to the four disulfide bonds. In addition, it can be found that the adsorptions of HFBI on different hydrophobic surfaces are driven by a few common residues located in the hydrophobic patch, that is, Leu12, Leu24, Leu26, Ile27, Ala66, and Leu68, indicative of a hydrophobicity-induced mechanism. The proposed adsorption mechanism results in a significant change of the hydrophobicity of the surface, which is supported by the previous experiment of water contact angle measurement.

It should be noted that HFBI exists in solution mainly as a tetramer to protect the hydrophobic patch of the protein. Close to a hydrophobic surface, the tetramer dissociates and adsorbs on the surface, forming a regular pattern via specific protein–protein interactions. Hence, the cooperative effects of protein–protein and protein–surface interactions on the adsorption are very important. On account of the complicated adsorption

process of multiproteins, only the adsorption behavior of single HFBI on the PDMS substrate was focused on in the present contribution. The results reported herein shed, nonetheless, meaningful light on the potential of hydrophobin adsorption for surface functionalization, in particular, changing the hydrophobicity of surfaces. On the basis of this preliminary investigation, the cooperative effects will be considered for our future computational explorations. An important issue about the immobilization of a second protein on the scaffold coated by hydrophobins may be addressed, which would further improve the understanding of the fundamental forces and process involved in the immobilization process.

■ ASSOCIATED CONTENT

Supporting Information

Details of the molecular systems and the simulations of the adsorption, monomers A and D, input files for the adsorption simulation with orientation 3, and analysis of the MD trajectories, including energies, structural stability, and flexibility, are provided. This material is available free of charge via the Internet at http://pubs.acs.org.

■ AUTHOR INFORMATION

Corresponding Author

*E-mail: wscai@nankai.edu.cn.

Notes

The authors declare no competing financial interest.

■ ACKNOWLEDGMENTS

This study was supported by the National Natural Science Foundation of China (Nos. 20873066 and 20835002) and the National Basic Research Program of China (No. 2011CB935904).

■ REFERENCES

(1) Wong, L. S.; Khan, F.; Micklefield, J. *Chem. Rev.* **2009**, *109*, 4025−4053.
(2) Linder, M.; Szilvay, G. R.; Nakari-Setala, T.; Soderlund, H.; Penttila, M. *Protein Sci.* **2002**, *11*, 2257−2266.
(3) Palomo, J. M.; Penas, M. M.; Fernandez-Lorente, G.; Mateo, C.; Pisabarro, A. G.; Fernandez-Lafuente, R.; Ramirez, L.; Guisan, J. M. *Biomacromolecules* **2003**, *4*, 204−210.
(4) Corvis, Y.; Walcarius, A.; Rink, R.; Mrabet, N. T.; Rogalska, E. *Anal. Chem.* **2005**, *77*, 1622−1630.
(5) Wang, Z. F.; Huang, Y. J.; Li, S.; Xu, H. J.; Linder, M. B.; Qiao, M. Q. *Biosens. Bioelectron.* **2010**, *26*, 1074−1079.
(6) Valo, H. K.; Laaksonen, P. H.; Peltonen, L. J.; Linder, M. B.; Hirvonen, J. T.; Laaksonen, T. J. *ACS Nano* **2010**, *4*, 1750−1758.
(7) von Vacano, B.; Xu, R.; Hirth, S.; Herzenstiel, I.; Ruckel, M.; Subkowski, T.; Baus, U. *Anal. Bioanal. Chem.* **2011**, *400*, 2031−2040.
(8) Aimanianda, V.; Bayry, J.; Bozza, S.; Kniemeyer, O.; Perruccio, K.; Elluru, S. R.; Clavaud, C.; Paris, S.; Brakhage, A. A.; Kaveri, S. V.; Romani, L.; Latge, J. P. *Nature* **2009**, *460*, 1117−1121.
(9) Kisko, K.; Szilvay, G. R.; Vuorimaa, E.; Lemmetyinen, H.; Linder, M. B.; Torkkeli, M.; Serimaa, R. *Langmuir* **2009**, *25*, 1612−1619.
(10) Paananen, A.; Vuorimaa, E.; Torkkeli, M.; Penttila, M.; Kauranen, M.; Ikkala, O.; Lemmetyinen, H.; Serimaa, R.; Linder, M. B. *Biochemistry* **2003**, *42*, 5253−5258.
(11) Hakanpaa, J.; Paananen, A.; Askolin, S.; Nakari-Setala, T.; Parkkinen, T.; Penttila, M.; Linder, M. B.; Rouvinen, J. *J. Biol. Chem.* **2004**, *279*, 534−539.
(12) Kurppa, K.; Jiang, H.; Szilvay, G. R.; Nasibulin, A. G.; Kauppinen, E. L.; Linder, M. B. *Angew. Chem., Int. Ed.* **2007**, *46*, 6446−6449.
(13) Kallio, J. M.; Rouvinen, J. *Chem. Commun.* **2011**, *47*, 9843−9845.
(14) Hektor, H. J.; Scholtmeijer, K. *Curr. Opin. Biotechnol.* **2005**, *16*, 434−439.
(15) Linder, M. B. *Curr. Opin. Colloid Interface Sci.* **2009**, *14*, 356−363.
(16) Laaksonen, P.; Kainlauri, M.; Laaksonen, T.; Shchepetov, A.; Jiang, H.; Ahopelto, J.; Linder, M. B. *Angew. Chem., Int. Ed.* **2010**, *49*, 4946−4949.
(17) Qin, M.; Wang, L. K.; Feng, X. Z.; Yang, Y. L.; Wang, R.; Wang, C.; Yu, L.; Shao, B.; Qiao, M. Q. *Langmuir* **2007**, *23*, 4465−4471.
(18) Zhou, J. W.; Ellis, A. V.; Voelcker, N. H. *Electrophoresis* **2010**, *31*, 2−16.
(19) Ouyang, M.; Yuan, C.; Muisener, R. J.; Boulares, A.; Koberstein, J. T. *Chem. Mater.* **2000**, *12*, 1591−1596.
(20) Wang, R.; Yang, Y. L.; Qin, M.; Wang, L. K.; Yu, L.; Shao, B.; Qiao, M. Q.; Wang, C.; Feng, X. Z. *Chem. Mater.* **2007**, *19*, 3227−3231.
(21) Latour, R. A. *Biointerphases* **2008**, *3*, Fc2−Fc12.
(22) Szott, L. M.; Horbett, T. A. *Curr. Opin. Chem. Biol.* **2011**, *15*, 683−689.
(23) Moldovan, C.; Thompson, D. *J. Mol. Model.* **2011**, *17*, 2227−2235.
(24) Mereghetti, P.; Wade, R. C. *BMC Biophys.* **2011**, *4*. DOI: 10.1186/2046-1682-4-9.
(25) Zangi, R.; de Vocht, M. L.; Robillard, G. T.; Mark, A. E. *Biophys. J.* **2002**, *83*, 112−124.
(26) Fan, H.; Wang, X. Q.; Zhu, J.; Robillard, G. T.; Mark, A. E. *Proteins* **2006**, *64*, 863−873.
(27) Hakanpaa, J.; Szilvay, G. R.; Kaljunen, H.; Maksimainen, M.; Linder, M.; Rouvinen, J. *Protein Sci.* **2006**, *15*, 2129−2140.
(28) Guex, N.; Peitsch, M. C. *Electrophoresis* **1997**, *18*, 2714−2723.
(29) Ismail, A. E.; Grest, G. S.; Heine, D. R.; Stevens, M. J.; Tsige, M. *Macromolecules* **2009**, *42*, 3186−3194.
(30) Phillips, J. C.; Braun, R.; Wang, W.; Gumbart, J.; Tajkhorshid, E.; Villa, E.; Chipot, C.; Skeel, R. D.; Kale, L.; Schulten, K. *J. Comput. Chem.* **2005**, *26*, 1781−1802.
(31) MacKerell, A. D.; Bashford, D.; Bellott, M.; Dunbrack, R. L.; Evanseck, J. D.; Field, M. J.; Fischer, S.; Gao, J.; Guo, H.; Ha, S.; et al. *J. Phys. Chem. B* **1998**, *102*, 3586−3616.
(32) Mackerell, A. D.; Feig, M.; Brooks, C. L. *J. Comput. Chem.* **2004**, *25*, 1400−1415.
(33) Jorgensen, W. L.; Chandrasekhar, J.; Madura, J. D.; Impey, R. W.; Klein, M. L. *J. Chem. Phys.* **1983**, *79*, 926−935.
(34) Bahar, I.; Zuniga, I.; Dodge, R.; Mattice, W. L. *Macromolecules* **1991**, *24*, 2986−2992.
(35) Smith, J. S.; Borodin, O.; Smith, G. D. *J. Phys. Chem. B* **2004**, *108*, 20340−20350.
(36) Schneemilch, M.; Quirke, N. *J. Chem. Phys.* **2007**, *127*, 114701−114707.
(37) Feller, S. E.; Zhang, Y. H.; Pastor, R. W.; Brooks, B. R. *J. Chem. Phys.* **1995**, *103*, 4613−4621.
(38) Tuckerman, M.; Berne, B. J.; Martyna, G. J. *J. Chem. Phys.* **1992**, *97*, 1990−2001.
(39) Ryckaert, J. P.; Ciccotti, G.; Berendsen, H. J. C. *J. Comput. Phys.* **1977**, *23*, 327−341.
(40) Andersen, H. C. *J. Comput. Phys.* **1983**, *52*, 24−34.
(41) Darden, T.; York, D.; Pedersen, L. *J. Chem. Phys.* **1993**, *98*, 10089−10092.
(42) Humphrey, W.; Dalke, A.; Schulten, K. *J. Mol. Graphics* **1996**, *14*, 33−38.
(43) Kollman, P. A.; Massova, I.; Reyes, C.; Kuhn, B.; Huo, S. H.; Chong, L.; Lee, M.; Lee, T.; Duan, Y.; Wang, W.; Donini, O.; Cieplak, P.; Srinivasan, J.; Case, D. A.; Cheatham, T. E. *Acc. Chem. Res.* **2000**, *33*, 889−897.
(44) Baker, N. A.; Sept, D.; Joseph, S.; Holst, M. J.; McCammon, J. A. *Proc. Natl. Acad. Sci. U.S.A.* **2001**, *98*, 10037−10041.
(45) Konecny, R. *iAPBS Interface on the Web*. http://mccammon.ucsd.edu/iapbs (accessed May 14, 2012).

(46) Askolin, S.; Linder, M.; Scholtmeijer, K.; Tenkanen, M.; Penttila, M.; de Vocht, M. L.; Wosten, H. A. B. *Biomacromolecules* **2006**, *7*, 1295−1301.
(47) Kyte, J.; Doolittle, R. F. *J. Mol. Biol.* **1982**, *157*, 105−32.
(48) Liu, Y. Z.; Cai, W. S.; Shao, X. G. *Chem. Res. Chin. Univ.* **2012**, *33*, 2013−2018.
(49) Sung, W. C.; Chang, C. C.; Makamba, H.; Chen, S. H. *Anal. Chem.* **2008**, *80*, 1529−1535.